An Essential Cytoskeletal Linker Protein Connecting Actin Microfilaments to Intermediate Filaments

Yanmin Yang,* James Dowling,* Qian-Chun Yu,* Panos Kouklis,* Don W. Cleveland,† and Elaine Fuchs*
*Howard Hughes Medical Institute
Department of Molecular Genetics and Cell Biology
The University of Chicago
Chicago, Illinois 60637
†Ludwig Institute for Cancer Research
Departments of Medicine and Neuroscience
University of California, San Diego
La Jolla, California 92093

Summary

Typified by rapid degeneration of sensory neurons, *dystonia musculorum* mice have a defective *BPAG1* gene, known to be expressed in epidermis. We report a neuronal splice form, BPAG1n, which localizes to sensory axons. Both isoforms have a coiled-coil rod, followed by a carboxy domain that associates with intermediate filaments. However, the amino terminus of BPAG1n differs from BPAG1e in that it contains a functional actin-binding domain. In transfected cells, BPAG1n coaligns neurofilaments and microfilaments, establishing this as a cytoskeletal protein interconnecting actin and intermediate filament cytoskeletons. In *BPAG1* null mice, axonal architecture is markedly perturbed, consistent with a failure to tether neurofilaments to the actin cytoskeleton and underscoring the physiological relevance of this protein.

Introduction

The 230 kDa epidermal form of bullous pemphigoid antigen 1 (BPAG1e), first identified with antisera from patients with the autoimmune disorder, bullous pemphigoid (BP; Stanley, 1993), belongs to a small group of large coiled-coil proteins that includes desmoplakin and plectin (Green et al., 1992). Both desmoplakin and plectin can associate with intermediate filaments (IFs) (Foisner et al., 1991; Stappenbeck and Green, 1992; Kouklis et al., 1994). While plectin decorates IF networks and is expressed ubiquitously, desmoplakin connects IFs to desmosomes in muscle and stratified epithelia. Similar studies have not yet been conducted with BPAG1e, although this protein localizes to the intracellular portion of the hemidesmosomal plaque, in a region where keratin filaments associate with the plaque (Stanley, 1993). Recent knockout studies revealed that basal epidermal cells lacking BPAG1e have hemidesmosomes with seemingly normal structure, but with severed connections to the keratin IF cytoskeleton (Guo et al., 1995).

Surprisingly, ablation of the *BPAG1* gene in mice (Guo et al., 1995) produced gross, rapid sensory neuron degeneration identical to *dystonia musculorum* (*dt*/*dt*), a well-known autosomal recessive mouse mutant (Duchen, 1976). While allelic with our *BPAG1* null mice, only one of two previously identified *dt*/*dt* mouse strains lacked BPAG1e, leading us to predict the existence of two forms of BPAG1, one expressed in epidermis and one in neurons (Guo et al., 1995). Additional evidence came from Brown et al. (1995a), who cloned the site of a 70 kb insertion/45 kb deletion from an *hsp70–lacZ* transgene random integration event that occurred within several hundred kilobases of the *BPAG1e* locus on mouse chromosome 1, creating a *dt*/*dt* phenotype (Kothary et al., 1988). These researchers isolated a partial brain cDNA that encoded 214 amino-terminal residues sharing similarity to the actin-binding domain (ABD) of β-spectrin and α-actinin. Whether this is a functional actin-binding site is unclear. Moreover, other researchers have previously isolated a partial cDNA encoding yet another form of BPAG1 protein (BPAG1t) that differs in its carboxy-terminal sequences (Hopkinson and Jones, 1994).

We were interested in the possible cytoskeletal interactions of BPAG1n as a means of understanding how the absence of BPAG1n can cause dramatic neurologic degeneration. As reported for *dt*/*dt* mice (Sotelo and Guenet, 1988), axons degenerate within the peripheral nervous system of 4-week-old *BPAG1* knockout mice (Guo et al., 1995). Severely affected are the large primary sensory axons, while more modest degeneration is seen in second order sensory neurons and in a few motor neurons. Studies on mouse chimeras composed of *dt*/*dt* and wild-type cells indicate that the defect is intrinsic (although not necessarily exclusively) to sensory neurons (Campbell and Peterson, 1992).

The extent to which BPAG1n shares sequences with BPAG1e or BPAG1t is key to deciphering why it is an essential protein. The carboxy-terminal portion of BPAG1e, missing in BPAG1t, is predicted to associate with keratin IFs. If BPAG1n contains this putative IF domain of BPAG1e, it might have the extraordinary capacity to bind simultaneously to both actin microfilaments (MFs) and IFs. On the other hand, if BPAG1n is missing this domain, it might differ completely from BPAG1e in its cytoskeletal associations. In this report, we determine the complete structure of BPAG1n protein and show that it has functional actin- and neurofilament (NF)-binding sites at opposite ends of its coiled-coil rod. Accumulating along the length of sensory axons, BPAG1n represents a novel class of cytoskeletal protein that serves a key in vivo role of linking actin and IF arrays. Our findings provide insights into the possible relation of recessive *BPAG1* mutations to severe human neurodegenerative disorders.

Results

The Brain Form of BPAG1 Contains the Complete Coding Sequence of BPAG1e, minus Exon 1

To identify the form of BPAG1 expressed in brain, we screened a human fetal brain cDNA library with a cDNA to exons 2–5 of the epidermal form of *BPAG1*. Five different cDNAs were identified. Rapid amplification of cDNA ends (RACE) completed the encoded amino-terminal segment. Sequencing revealed the existence of

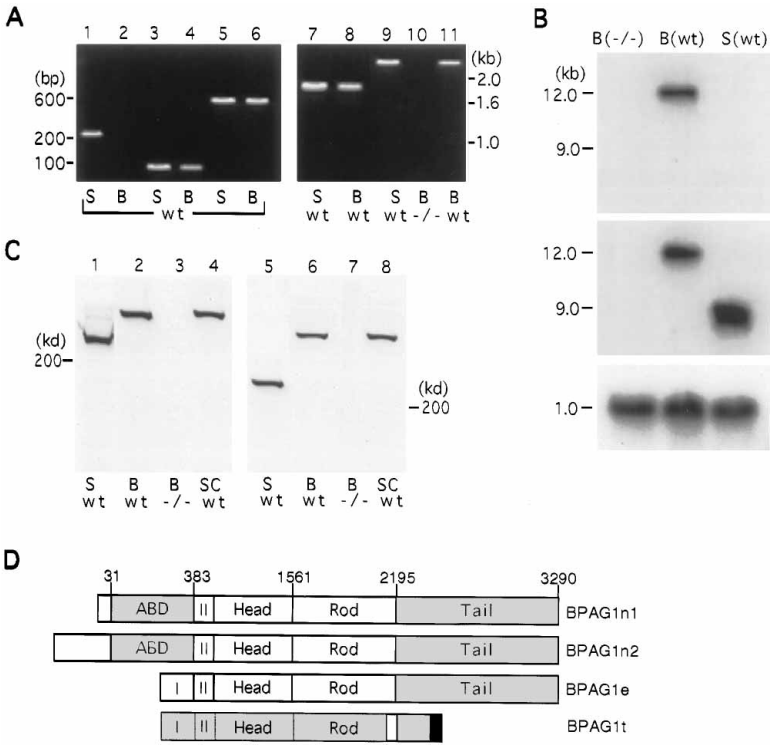

Figure 1. Elucidating the Complete Structure of *BPAG1n* mRNA and Protein

(A) PCR analysis of mouse and human skin and brain *BPAG1* mRNAs. Total RNAs were isolated from skin (S) and brain (B) tissues of human or 14-day-old wild-type (wt) and *BPAG1* null (−/−) mice. Oligonucleotide primers were used to PCR amplify mouse and human *BPAG1* sequences, and DNA fragments were resolved by agarose gel electrophoresis (2% left gel; 1% right gel) and visualized by ethidium bromide staining. Shown are mouse data. Fragments encompassed are as follows: lanes 1 and 2, exons 1 and 2 of *BPAG1e*; lanes 3 and 4, exon 2 of *BPAG1e*; lanes 5 and 6, β-actin cDNA (control); lanes 7 and 8, exons 15–21, which comprise the coiled-coil rod of BPAG1e; and lanes 9–11, the nonhelical tail of BPAG1e. Migration of DNA standards are indicated at left and right.

(B) Northern blot analysis of mouse skin and brain *BPAG1* mRNAs. Poly(A)$^+$ RNAs (2 μg) were resolved by electrophoresis through formaldehyde–agarose gels (0.6%). RNAs were transferred by blotting to nitrocellulose, and blots were hybridized with ^{32}P-labeled cDNA probes against (top) a 680 bp mouse *BPAG1n* cDNA corresponding to the 5′ coding segment unique to *BPAG1n*, (middle) a 1.2 kb mouse *BPAG1e* cDNA spanning parts of exons 21 and 22 (3′ coding segment), or (bottom) a 1 kb mouse glyceraldehyde phosphate dehydrogenase (GAPDH) cDNA (control). Migration of RNA standards is indicated at left.

(C) Immunoblot analysis of skin (S), brain (B), and spinal cord (SC) proteins isolated from (−/−) and wild-type mice. Protein extracts in 20 mM Tris–HCl (pH 7.5), 1% Triton X-100, 0.1% SDS, 5 mM EDTA were resolved by electrophoresis through 6% SDS–polyacrylamide gels and then transferred to nitrocellulose by electroblotting. Blots were stained with Ponceau red (data not shown) to examine relative loadings and then subjected to immunoblot analysis with (left) m5E monoclonal antibody against a BPAG1 tail epitope (1:500 dilution) and (right) anti-BPAG1n (1:1000 dilution). Horseradish peroxidase secondary antibodies and chemiluminescence were used to develop the signal. Migration of muscle myosin (200 kDa) control is shown. Note single BPAG1n band, despite the existence of two isoforms based on cDNA analysis.

(D) Diagram of four human BPAG1 isoforms. Shown are protein structures of two BPAG1n isoforms, determined from amino acid 1 through exon 2 (II) of BPAG1e by Brown et al. (1995a, 1995b) and assessed in their entirety here. Numbers at top represent amino acids of the BPAG1n1 sequence. Shown also is the complete protein structure of human BPAG1e, with a unique exon 1 (I) determined by Tamai et al. (1993), and the hypothesized structure of the 280 kDa human pancreatic BPAG1t, partially cloned as a putative tailless BPAG1 (Hopkinson and Jones, 1994).

two transcripts that differ in their 5′ sequence, encoding a divergent initial 31 (for BPAG1n1) and 215 (for BPAG1n2) amino acids, followed by 352 shared residues prior to amino acid residue 55 of BPAG1e. These two brain forms matched with recently published 5′ segments of human brain *BPAG1n* cDNA (Brown et al., 1995b). To identify the more carboxy-terminal structures of the two brain BPAG1s, reverse transcriptase–polymerase chain reaction (RT–PCR) of isolated mouse brain RNA was used to amplify the coding segments of *BPAG1n1* and *BPAG1n2* mRNAs (Figure 1A). Oligonucleotide primers spanning exons 1 and 2 of *BPAG1e* amplified a band only in skin and not in brain. In contrast, primer pairs within exon 2 generated a band in both skin and brain. Similar data were obtained with human RNAs (data not shown). Collectively, these results verified the existence of human and mouse RNAs encoding the cloned *BPAG1n* cDNAs, and revealed that the BPAG1e form is not expressed in brain.

To determine the remainder of the BPAG1n1 and BPAG1n2 sequences, we used oligonucleotide primer sets encompassing BPAG1e, including the ~625 amino acid residue coiled-coil "rod" (exons 16–20) and the 768 residue "tail" (exons 21 and 22) (Tamai et al., 1993). In all cases, PCR bands were generated from skin and brain RNAs; these bands were not present in RNAs from *BPAG1* (−/−) knockout mice. Sequence analyses of the isolated cDNA clones showed that the encoded 1103 amino acid "head" (exons 2–15) was present in both BPAG1n1 and BPAG1n2. Sequence analyses of the PCR fragments confirmed that the remaining exons of *BPAG1e* (exons 15–22) are present in brain RNAs.

Northern blot analysis demonstrated the existence of a 12 kb brain *BPAG1n* RNA(s) hybridizing to radiolabeled probes to the 5′ and 3′ sequences common to both *BPAG1n* isoforms (Figure 1B). This RNA was not detected in whole skin preparations or in brain tissue from *BPAG1* knockout mice (−/−). Thus, the 12 kb *BPAG1n* mRNA is not appreciably expressed in skin, in contrast with prior predictions based on detection of a *BPAG1*-related RNA in a cultured epithelial line (Brown et al., 1995a).

The ~280 kDa BPAG1n Protein Is Present in Brain and Spinal Cord

To verify the existence of BPAG1n protein, immunoblots of extracts from skin, brain, and spinal cord were probed with a monoclonal antibody (E5a) made from a BP patient autoantisera and recognizing an epitope in the BPAG1e tail segment (Sugi et al., 1989). In addition to binding to the 230 kDa BPAG1e band in skin, this antibody detected a 280 kDa band in brain and spinal cord (Figure 1C). That this band corresponds to BPAG1n was confirmed by probing a second blot with a rabbit antiserum prepared against the putative ABD of BPAG1n fused to glutathione S-transferase (GST). We conclude that a single protein contains the carboxy-terminal sequence common to skin and brain BPAG1 isoforms as well as the amino-terminal sequence encoded by the brain cDNAs. The size of the BPAG1n band corresponded to that predicted for BPAG1n1, although the antibody should have detected both isoforms with equal affinity. A minor band of ~250 kDa was also detected (see lane 1 of Figure 1C); its identity remains unknown.

Figure 1D summarizes the structure of BPAG1n1 and BPAG1n2 relative to other BPAG1 forms. Since *dystonia musculorum* does not appear to be a bona fide model of human dystonia, and since both brain and skin BPAG1s are antigenic determinants of BP autoantisera, we have kept the nomenclature first set for the epidermal form, and henceforth we refer to the 280 kDa band detected in Figure 1C as BPAG1n.

BPAG1n Is Expressed Primarily in Sensory Neurons

To examine the role of BPAG1n in the central and peripheral nervous system, we first used in situ hybridization to determine where *BPAG1n* mRNAs are expressed. As shown in Figure 2A and viewed at higher magnification in Figure 2B, the perikarya of the dorsal root ganglia (DRG) neurons of neonatal mice hybridized with didegoxygenin-labeled, *BPAG1n*-specific cRNA. When compared with a *trkC* probe, which labeled the 1a afferent subset of primary sensory neurons (Figure 2C), it was clear that *BPAG1n* mRNAs were expressed more widely within the sensory neuron population (Figure 2B). The smaller satellite cells within the DRG did not appear to label with the probe (arrows in inset to Figure 2B), nor did cells of the *BPAG1* knockout mice (data not shown). Moreover, in contrast with the *BPAG1n* cRNA labeling in the DRG, neither the spinal cord, sensory roots, nor peripheral nerves gave labeling above background. Collectively, our data demonstrated, first, the existence of *BPAG1n* RNAs in most if not all postnatal DRG neurons and, second, little if any labeling in postnatal motor neurons, satellite cells, oligodendrocytes, or Schwann cells.

To determine the location of BPAG1n within sensory neurons, anti-BPAG1n antiserum was used for immunogold immunohistochemistry on postnatal central and peripheral nervous system tissue sections (Figure 3). As judged by antibody labeling, BPAG1n protein did not appear to remain in DRG cell bodies where its mRNA was produced; rather anti-BPAG1n staining was prominent in axonal rootlets (Figures 3A and 3B). Relative to the unlabeled spinal cord of the *BPAG1* null mouse

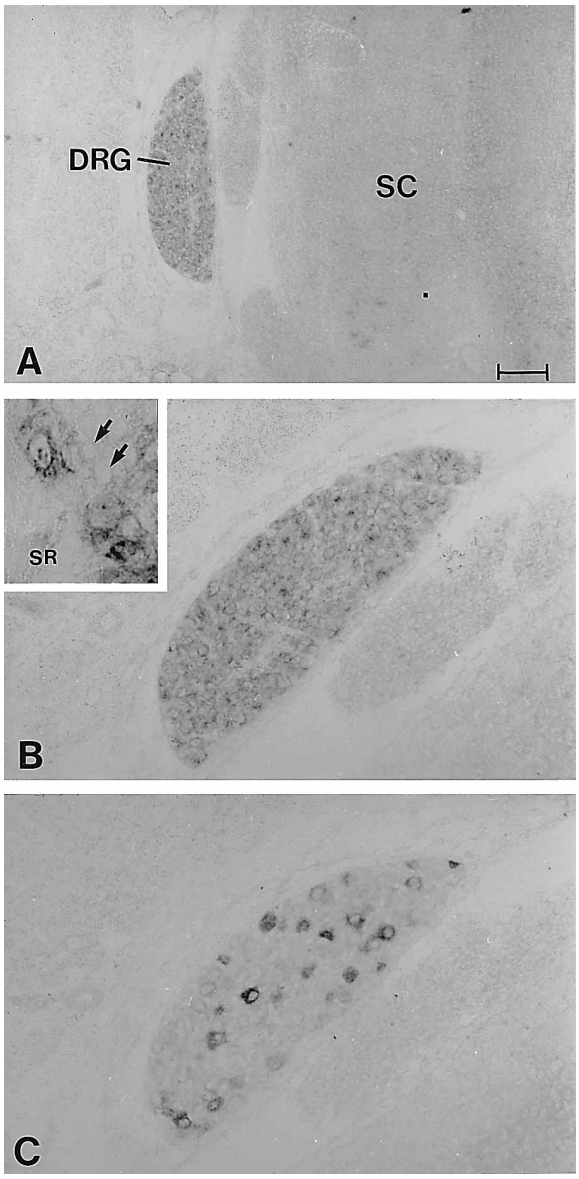

Figure 2. In Situ Hybridizations Reveal Abundant and Specific Expression of *BPAG1n* RNA in All Primary Sensory Neurons of the DRG

In situ hybridizations were performed on frozen transverse sections from postnatal day 1 mice according to Yang et al. (1996). Hybridizations using didegoxygenin (DIG) cRNAs were performed for 16 hr at 72°C, followed by stringent washes for 3 hr at 72°C in 0.2× SCC. Colorimetric detection was by an alkaline phosphatase–conjugated goat anti-DIG antibody (1:5000 dilution; Boehringer Mannheim).

(A) Cross section of spinal cord hybridized with probe specific for a 543 bp (nucleotides 699–1242) fragment of mouse *BPAG1n2*.

(B) Higher magnification of region in (A), showing DRG-specific hybridization; inset shows labeling of larger sensory cell bodies, but not smaller satellite cells (similar to Schwann cells; arrows). SR, senory root.

(C) DRG labeled with DIG probe specific for a 433 bp fragment of the *trkC* receptor cDNA (Minichiello et al., 1995), present in a subset of sensory neurons within the DRG.

Bar in (A) represents 150 μm in (A); 80 μm in (B) and (C); and 15 μm in the inset.

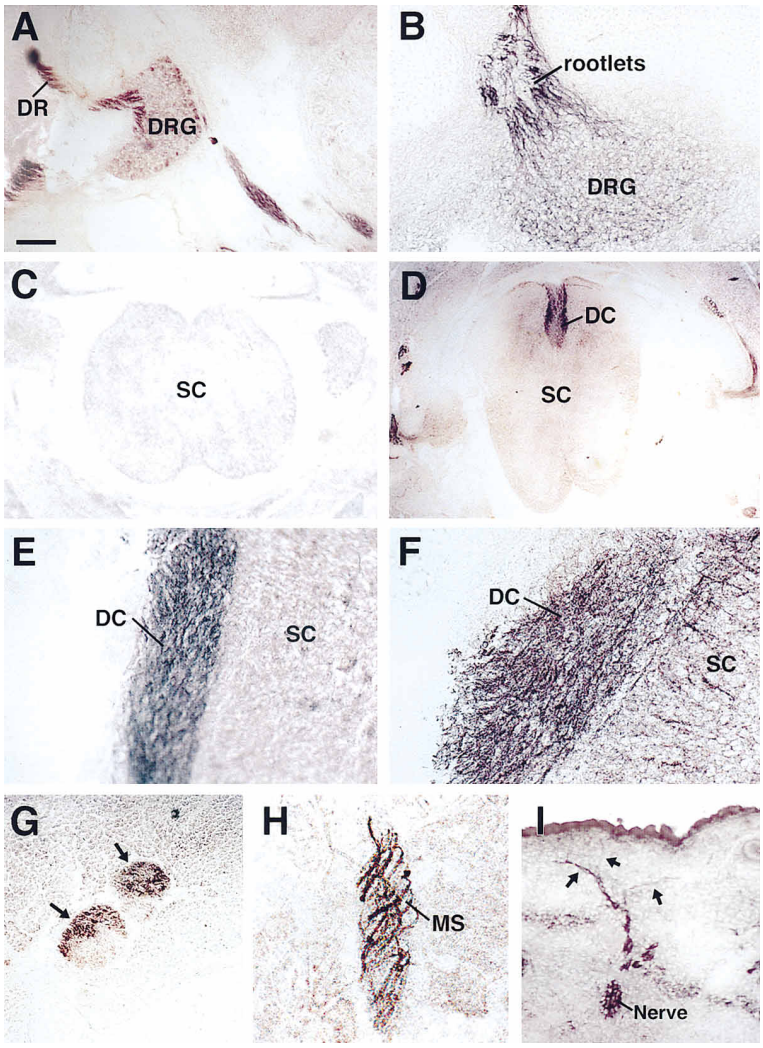

Figure 3. Immunohistochemistry Reveals of BPAG1n in the Axons and Preterminal Branches of the Sensory Neurons of the Peripheral and Central Nervous System

Frozen tissue sections (20 μm) of brain, spinal cord, and skin were taken from wild-type (A, B, and D–I) and *BPAG1* null (C) mice at 12 days after birth. Sections were treated with methanol (−20°C) for 10 min, washed three times with phosphate-buffered saline (PBS), preblocked with 1% BSA, 0.1% Triton X-100, and 1% gelatin in PBS, and then exposed to anti-BPAG1n (1:100 dilution) at room temperature overnight. After washing three times with PBS for 10 min each, sections were incubated with secondary antibody (1:50 dilution) conjugated with immunogold for 30 min, and then washed and mounted. Sections were examined using a Zeiss Axiophot immunofluorescence microscope. All signals shown were specific for BPAG1n and were not seen in *BPAG1* (−/−) sections.

(A) Sagittal segment of spinal cord, revealing reduced staining in DRG perikarya relative to axonal rootlets. DR, dorsal root.

(B) A closer view of a DRG.

(C) Cross section of (−/−) spinal cord (SC).

(D) Cross section of spinal cord to show staining in dorsal column (DC).

(E and F) Sagittal views to show labeling of nerve fibers in dorsal column.

(G) Cross section of sciatic nerve (arrows), revealing staining in region closest to arrows.

(H) Muscle spindle (MS).

(I) Sensory nerve endings in skin; note labeling of termini (arrows).

Bar in (A) represents 16 μm in (A), (E), (G), and (I); 8 μm in (B) and (F); 60 μm in (C) and (D); and 4 μm in (H).

(Figure 3C), axons within the dorsal column of wild-type mice were strongly positive (Figure 3D). Sagittal sections of dorsal column revealed staining along its length (Figures 3E and 3F). Closer inspection of this region showed that the staining was specific for sensory nerve fibers (Figure 3F).

In contrast with the immunoreaction in the dorsal column, the ventral portion of the spinal cord displayed little or no detectable staining with anti-BPAG1n (Figure 3D), a finding expected from the absence of *BPAG1n* RNAs in similar sections (Figure 2A). These data argue that the majority of motor dysfunction in the *BPAG1* knockout mice is secondary. Consistent with this notion is that the sciatic nerve, which contains a mixture of motor and sensory axons, displayed some axons that stained with anti-BPAG1n and others that did not (Figure 3G).

Anti-BPAG1n staining was also detected in muscle spindles, the stretch receptors in skeletal muscle that are innervated by sensory nerve terminals from the DRG as well as motor neurons (Figure 3H). BPAG1n antibody staining was also found in the sensory nerve termini within skin (Figure 3I). The epidermal labeling was likely due to the ability of the antibody to detect *BPAG1* exon 2, present in both BPAG1e and BPAG1n. Axons in the spinocerebellar tract also stained positive for BPAG1n (data not shown). These secondary nerve fibers serve as important sensory relays to the brain, where they deliver signals that originate from primary sensory fibers coming from muscle. Thus, expression of BPAG1n was not restricted to primary sensory neurons, but extended to some secondary sensory neurons.

Our findings are consistent with the pathology of the *BPAG1* knockout and *dt/dt* mice, but they differ markedly from the predictions of BPAG1n expression inferred from following expression of a *hsp70–lacZ* transgene integrated into the *BPAG1* locus in a *dt/dt* mouse mutant (Kothary et al., 1988).

The BPAG1 Tail Associates with IF Networks

The carboxy-terminal tail of desmoplakin associates with epidermal keratin networks in vivo (Kouklis et al., 1994). Given 40% amino acid sequence identity between an ~300 residue portion of the tails of desmoplakin and BPAG1 (Green et al., 1992), and given the finding that ablation of BPAG1e severs the connection between keratin IFs and hemidesmosomes (Guo et al., 1995), we tested whether the BPAG1 tail might have the capacity

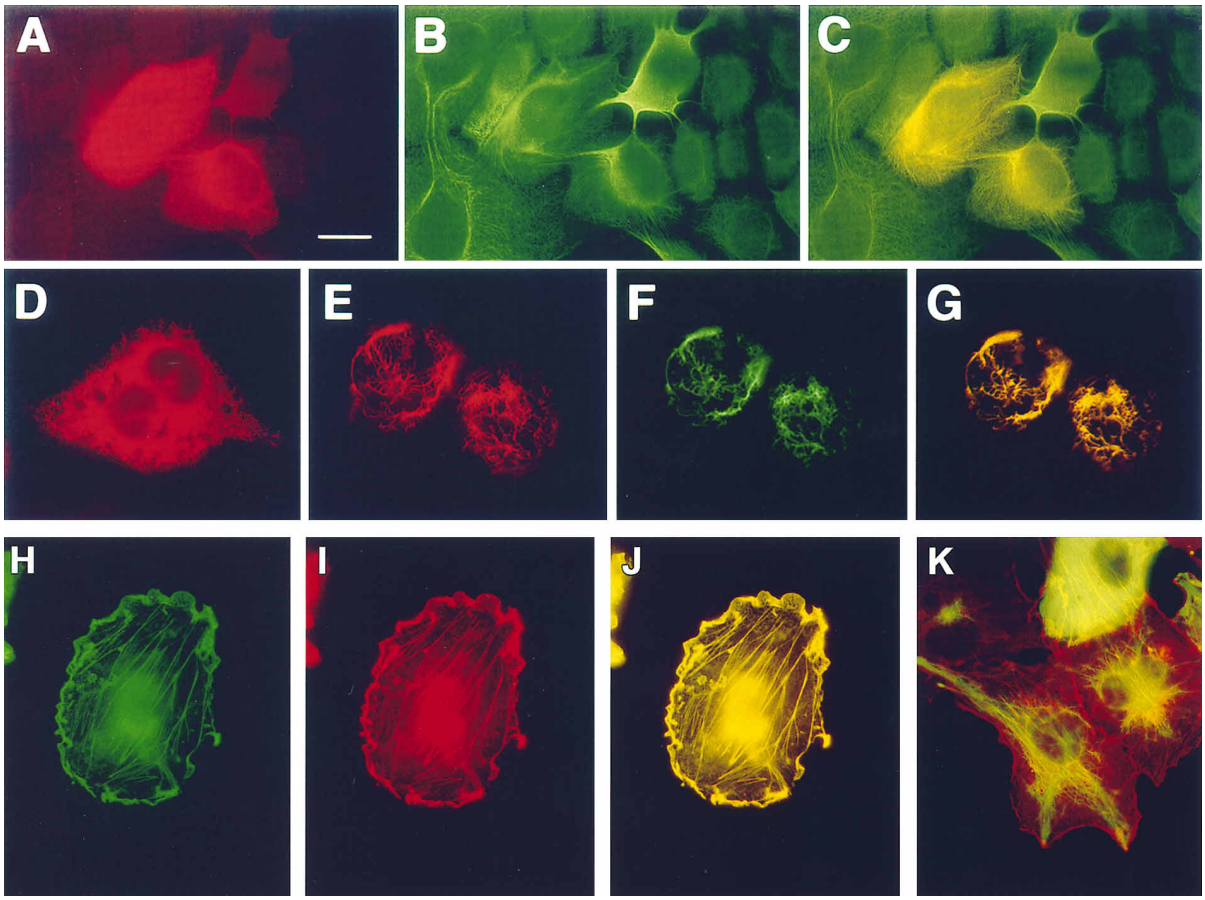

Figure 4. The Carboxy-Terminal Tail of BPAG1 Decorates IF Networks, and the Amino-Terminal Domain of BPAG1n Colocalizes with Actin Networks

SCC-13 human epidermal keratinocytes (keratin IF positive [A–C]) and SW13 human adrenal carcinoma cells (IF negative [D–K]) were transiently transfected with pFG-BPAG1tail alone (A–D), pBPabd-FG alone (H–J), or with a 1:1:1 molar ratio of murine sarcoma virus–NF-L expression vector (MSV-NFL), MSV-NFH, and either pFG-BPAG1tail (E–G) or pBPabd-FG (K). After 28 (SCC-13) or 36 hr (SW13), cells were fixed and subjected to double immunofluorescence as described previously (Albers and Fuchs, 1987). Transfected cells were stained with the following: (A), (D), (E), and (I), mouse anti-FLAG M2 monoclonal antibody (10 μg/ml; IBI-Kodak); (B), anti-K5, against an epidermal keratin; (F), affinity-purified rabbit anti-NF-H polyclonal antisera (1:300); (C), guinea pig anti-K5 (1:100; Lersch et al., 1989)/anti-FLAG; (G) and (K), anti-NF-H/anti-FLAG; (H), mouse monoclonal β-actin antibody (1:100; Sigma); (J), anti-actin/anti-FLAG. Appropriate FITC- and Texas red–conjugated secondary antibodies were used to detect bound antibodies. Bar represents 16 μm for (A)–(G) and (K) and 10 μm for (H)–(J).

to associate with IF networks. The entire 768 residue tail of human BPAG1n/e, tagged at its amino terminus with a small epitope (FLAG), was expressed transiently in SCC-13 keratinocytes. The BPAG1 tail decorated the epidermal IF network (Figures 4A–4C), which in the majority of transfected cells was unaffected by the transgene product.

When expressed in the SW13 cell line lacking cytoplasmic IFs, the BPAG1 tail accumulated diffusely in the cytoplasm, devoid of a filamentous appearance (Figure 4D). An immunofluorescence signal could only be seen at early timepoints after transfection (e.g., 24 hr), suggesting that the protein is unstable in this cell line. In contrast, when an extensive array of NFs was produced in vivo by cotransfection with a 1:1 ratio of NF-L (light chain) and NF-H (heavy chain) expression vectors (Lee et al., 1993), the BPAG1 tail decorated the cytoskeletal array of NFs (Figures 4E–4G). In this case, the anti-FLAG immunofluorescence signal was strong even at 40 hr posttransfection, implying that the BPAG1 tail is stabilized by binding to an IF array.

To verify that the association between BPAG1 tail and NFs was specific, transfections were repeated in monkey kidney epithelial (COS) cells that harbor the simian virus 40 (SV40) T antigen, resulting in amplification of the transfected plasmids. Following transfection, cell extracts were prepared and first subjected to immunoblot analyses to verify that the proteins were stably expressed and of the expected size. As shown in Figure 5A, the ~80 kDa BPAG1 tail protein accumulated, as did NF-L (~70 kDa), NF-H (~200 kDa), and full-length BPAG1n (280 kDa).

To examine the specificity of the association between the BPAG1 tail segment and NFs, we transfected COS cells with the BPAG1 tail or NF-H constructs (or both) and incubated the cells in the presence of medium containing [^{35}S]methionine. After 28 hr, extracts were subjected to immunoprecipitation with antibodies against

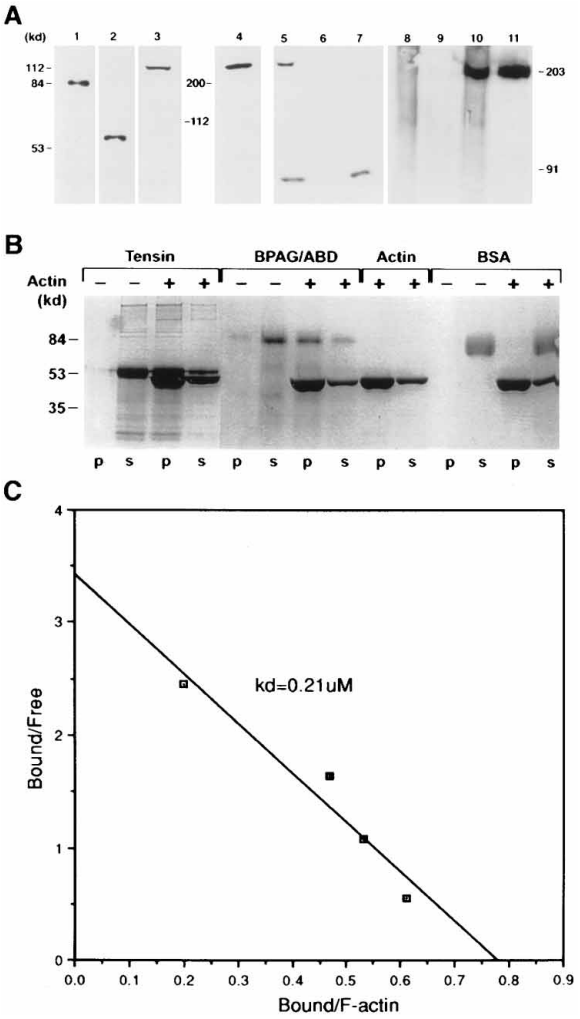

Figure 5. The BPAG1 Tail Forms a Complex With NF-H, and the BPAG1 Head Binds to Actin MFs

(A) COS cells were transfected with either pFG-BPAG1tail (lane 1), MSV-NFL (lane 2), a 1:1 molar mixture of MSV-NFL and MSV-NFH (lane 3), or pBPAG1n (lane 4). We lysed cells 36 hr after transfection and resolved total proteins by electrophoresis through 10% or 6% SDS–polyacrylamide gels. Following transfer to nitrocellulose, blots were first stained with Ponceau red to verify equal loading of protein (data not shown) and then subjected to immunoblot analysis with anti-FLAG (lane 1), anti-NF-L (lane 2), anti-NF-H (lane 3), or anti-BPAG1n (lane 4). After washing, the blots were developed using enhanced chemiluminescence. Note the presence of a single band of the expected size for each of the cell extracts. COS cells were also radiolabeled with 10 μCi/ml [^{35}S]methionine (1 Ci/mmol; Amersham) following transfection with a 1:1 molar ratio of pFG-BPAG1tail and MSV-NFH (lane 5), MSV-NFH (lane 6), or pFG-BPAG1tail (lane 7). After 28 hr, cells were processed for immunoprecipitation with anti-FLAG antibody in 20 mM Tris–HCl (pH 7.5), 1% Triton X-100, 0.1% SDS, 5 mM EDTA. Following electrophoresis, the gel was subjected to autoradiography and exposed to X-ray film for 17 hr. Note that in the presence of BPAG1 tail, NF-H is selectively immunoprecipitated by anti-FLAG; vimentin (57 kDa), which also associates with the BPAG1 tail, is outside the size range necessary to visualize NF-H and BPAG1 tail. Finally, unlabeled COS cells were transfected, and immunoprecipitations were conducted. Following electrophoresis, proteins were transferred to nitrocellulose, and the blot was probed with anti-NF-H and processed. Transfections and antibodies used for immunoprecipitations were as follows: lane 8, pFG-BPAG1tail, anti-FLAG; lane 9, MSV-NFH, anti-FLAG; lane 10, MSV-NFH plus pFG-BPAG1tail, anti-FLAG; lane 11, MSV-NFH, anti-NF-H.

the FLAG-tagged BPAG1 tail. As judged by SDS–polyacrylamide gel electrophoresis and autoradiography, a band of the expected size of NF-H selectively associated with the 80 kDa BPAG1 tail and was coimmunoprecipitated with the antibody (Figure 5A). Immunoblot analysis of unlabeled COS cell extracts confirmed that this ~200 kDa band was indeed NF-H. The stoichiometry of the association was ~1:1, when size and methionine content were considered and when the radioactivity in the bands was quantitated. When expressed by itself, NF-H remained in the soluble fraction of detergent-containing cell extracts immunoprecipitated with anti-BPAG1n. However, following cotransfection, BPAG1 antibody immunoprecipitated NF-H nearly as efficiently as the NF-H antibody, confirming the association between the two proteins.

The Amino-Terminal Domain of BPAG1n Binds Actin Filaments In Vivo and In Vitro

The location of anti-BPAG1n labeling within the axon, coupled with the presence of a putative ABD in the amino-terminal portion of BPAG1n, suggested that BPAG1n might be tethered to the cytoskeleton of actin MFs known to be present in the axon (Hirokawa, 1982; Fath and Lasek, 1988). To assess whether this domain has the capacity to associate with the actin cytoskeleton, we used DNA transfection to express the amino-terminal portion of BPAG1n1 in SW13 cells. As shown in Figures 4H–4J, antibodies against BPAG1n and β-actin colocalized along the actin stress fibers and at the cortical actin cytoskeleton underlying the plasma membrane of these cells. Greater than 80% of the transfected cells displayed this phenotype. This portion of BPAG1n did not localize with NFs in cotransfected cells (Figure 4K).

To explore further the specificity of the amino-terminal domain of BPAG1n for actin filaments, polymerized actin was combined with GST–BPAG1n fusion protein (100 nM) encompassing this domain. As a control, we used a recombinant chicken tensin–GST fusion protein, con-

(B) Actin binding assays. Binding assays were conducted as described by Lo et al. (1994) to test the following: the ABD II of chicken tensin fused to GST (tensin; purified from p23-expressing cells; Lo et al., 1994); the ABD sequence of human brain BPAG1n fused to GST (BPAG/ABD); bovine serum albumin control (BSA); and GST protein control (data not shown). In brief, proteins (80 μg/ml) in P buffer (10 mM imidazone [pH 7.0], 75 mM KCl, 0.2 mM EGTA, 0.01% NP-40) were subjected to precentrifugation in a Beckman Airfuge to remove any aggregates and then combined with purified rabbit skeletal muscle F-actin (300 μg/ml in 0.2 mM ATP). After incubation (1 hr at room temperature), samples were subjected to centrifugation (100,000 × g for 40 min) to pellet the F-actin and its associated proteins. Fractions were then separated by electrophoresis through 8.5% SDS–polyacrylamide gels, which were then stained with Coomassie blue to visualize protein. The amounts of protein in the supernatant (S) or actin-containing pellet (P) were determined by densitometric scanning. Each assay was performed with (+) and without (−) polymerized actin filaments.

(C) Estimation of the K_d of actin binding. Actin filament binding assays were carried out as in (B), except that BPAG1n fusion protein was used at 100 nM, 200 nM, 300 nM, and 400 nm. Scatchard analysis was conducted on two data sets, which were averaged (values differed by less than 10%). Plot shown gives, on the vertical axis, BPAG1n bound/free BPAG1n μM^{-1}, and on the horizontal axis, bound BPAG1n/F-actin.

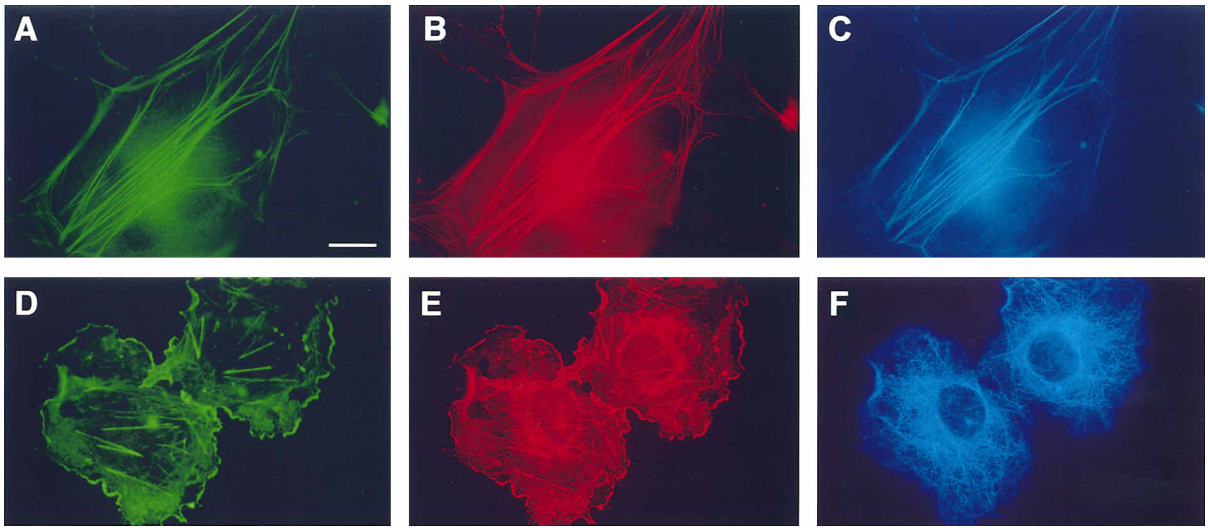

Figure 6. The Full-Length BPAG1n Can Reorganize an NF Network to Colocalize with the Actin Network in SW13 Cells

SW13 cells were transfected with a 1:1:1 molar ratio of MSV-NFL, MSV-NFH, and pBPAG1n1. Transfected cells were subjected to triple immunofluorescence in (A)–(C) with anti-NF-H (1:300, rabbit polyclonal), m5e (BPAG1; 1:50, human monoclonal), and anti-βactin (1:100, mouse monoclonal), respectively; in (D)–(F), anti-βactin, m5e (BPAG1), and anti-tubulin (1:100, rabbit polyclonal against tyrosinylated form), respectively. Appropriate FITC-, Texas red–, or Fluoroblue-conjugated secondary antibodies were used to detect bound antibodies. Shown are representative cells from each immunofluorescence staining. Bar in (A) represents 12 μm for all frames.

taining a bona fide ABD (Lo et al., 1994). In the absence of polymerized actin, neither ABD pelleted by centrifugation at 100,000 × g (Figure 5B). In contrast, addition of polymerized actin resulted in a major portion of the ABD now pelleting with actin. That these associations were specific to ABD-containing proteins was underscored by the failure of serum albumin or GST alone to shift to the pelletable fraction in this assay (see also Lo et al., 1994, and references therein). Note that some actin did not pellet, but the relative percentage of actin that remained in solution was constant irrespective of whether an ABD was added to the polymerized preparation. This presumably was reflective of unpolymerized actin.

To estimate the binding constant of this association, we repeated these experiments, this time using a range of BPAG1n concentrations from 100 nm to 400 nm. As expected, as the concentration of BPAG1n increased, the association of BPAG1n with polymerized actin became saturating, and the level of BPAG1n in the soluble fraction increased. A Scatchard plot of the data is shown in Figure 5C. The K_d of BPAG1n binding to actin was 2.1×10^{-7} M, within the range of that observed for β-spectrin and other proteins with ABDs (Lo et al., 1994).

Full-Length BPAG1n Has the Remarkable Capacity to Coalign Actin and NF Networks

In view of the ABD at one end of the coiled-coil rod segment of BPAG1n and an NF-binding domain at the other end, we examined the ability of these associations to take place simultaneously. In this case, we constructed a full-length cDNA for the 280 kDa BPAG1n and expressed it by DNA transfection. By immunoblot analysis, a band of the expected size was produced (Figure 5A, lane 4). When NF-L, NF-H, and BPAG1n were cotransfected into SW13 cells, NFs were formed that labeled with antibodies against NF-H (Figure 6A). However, in contrast with what we had observed in cotransfections with the BPAG1 tail domain, this NF network coaligned with the actin stress fiber network (Figure 6C). This association between the two cytoskeletal networks involved BPAG1n (Figure 6B). The actin network, anchored to the cortical cytoskeleton and to focal contacts, appeared less affected than the NFs, which are free in the cytoplasm of SW13 cells transfected with NF-L and NF-H alone. Approximately 20% of triple transfected cells showed complete colocalization of all three antibodies, 50% showed partial colocalization, and ~30% of the cells overexpressed one or more of the transgene proteins and therefore could not be categorized. Only a small percentage (<5%) of cells expressing BPAG1n displayed distinct actin and NF networks.

The association of the actin and NF networks in SW13 cells expressing BPAG1n did not appreciably affect the microtubule cytoskeleton. As shown in Figures 6D–6F, the cytoskeleton formed among actin, BPAG1n, and NFs did not colocalize with the microtubule network. Thus, if there are associations between BPAG1n and microtubules, these associations were not detected under the conditions used here.

Abnormalities in the Neurofilament Architecture in *BPAG1* Knockout Mice

In view of the reorganization of the NF network in SW13 cells cotransfected with BPAG1n, we reexamined the pathology of the *BPAG1* knockout animals to assess whether the NF network within sensory axons might be altered when BPAG1n is missing. First, we used the mouse monoclonal antibody SMI 31, which detects NF-H when it is multiphosphorylated within its lysine-serine-proline repeats in the tail (Sternberger and Sternberger, 1983). This antibody reacts broadly with axons,

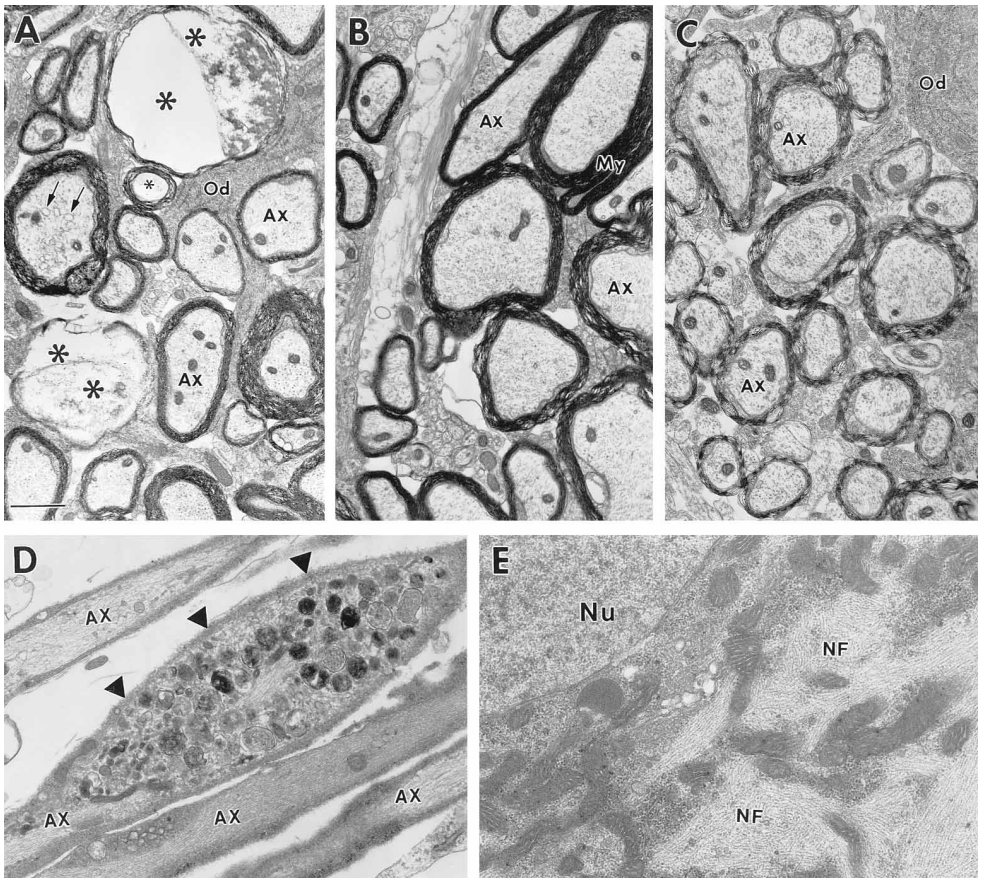

Figure 7. Ultrastructure of *BPAG1* Mutant Mice Reveals Signs of Nerve Fiber Degeneration in the Dorsal Column and Sensory Axons

BPAG1 (−/−) mice and control littermates at 12 days of age were perfused with a solution of 2% glutaraldehyde and 4% paraformaldehyde, and tissues were embedded in Epon. Tissues were processed as previously described (Coulombe et al., 1991) and examined with a Jeol 100 CX electron microscope at 80 kv. Shown are cross sections of the dorsal column of the spinal cord of *BPAG1* (−/−) (A) and control (B) mice and the ventral column of the spinal cord of *BPAG1* (−/−) mice (C). Shown also are axons (D; axonal swelling with lysosomal vesicles denoted by arrowheads) and cell body (E; note high density of NFs) from (−/−) DRG. Abbreviations are as follows: Ax, axon; My, myelinated sheath; asterisks, signs of degeneration; arrows, early degeneration; Od, oligodendrocyte. Varying stages of degeneration are evident within ~40% of the (−/−) axons of the dorsal column, but not within the ventral column. By 28 days (data not shown), >90% of the sensory neurons are degenerated, and eventually signs of degeneration, presumably secondary, are seen within the ventral column. Bar represents in (A) 0.8 μm in (A)–(C); 0.9 μm in (D); and 0.5 μm in (E).

but nerve cell bodies are unreactive. In contrast, many cell bodies of the *BPAG1* (−/−) DRG were labeled (data not shown). Similar aberrations have been described in certain degenerative disorders of motor neurons where NFs accumulate in perikarya (Xu et al., 1993; Cote et al., 1993).

Electron microscopy was used to examine the NF network in 12d *BPAG1* (−/−) sensory axons in greater detail. Approximately 30% of the axons in the dorsal column of the spinal cord were degenerated (Figure 7A), a number which would rise to >90% by 4–5 weeks of age (Guo et al., 1995). In contrast, the ventral root, housing motor axons emerging from the (−/−) spinal cord, was largely unaffected (Figure 7C).

Inspection along the length of the DRG axons revealed regional swellings filled with lysosomal vesicles and disorganized arrays of neurofilaments (Figure 7D). Both myelinated and nonmyelinated fibers seemed to be affected. Axonal degeneration was also accompanied by a reduction of NFs. In the dorsal column, there was an average of 56% ± 17% difference in NF density per unit area of axon cytoplasm. The initial reduction in NF density seemed most prominent in areas close to the axonal membrane. Accompanied by a reduction and disorganization of NFs in axons was an accumulation of NFs in cell bodies (Figure 7E).

Discussion

A Novel Kind of Cytoskeletal Connector: Linking Actin and IFs

Our biochemical and molecular analyses indicate that both neuronal isoforms of BPAG1 have the capacity to bind simultaneously to the actin and IF cytoskeletons. An ABD, not present in BPAG1e, resides at the amino end of the coiled-coil rod. Its binding to polymerized actin is with an affinity comparable with, if not stronger than, that of the well-established actin binding activity of tensin (Lo et al., 1994). At the carboxy end of the rod is an IF-binding domain, present in both BPAG1e and

BPAG1n. In keratinocytes, this domain associates with the keratin cytoskeleton, and in sensory neurons it binds to NFs.

Most remarkable is the ability of full-length BPAG1n to realign NFs in relation to the actin cytoskeleton in transfected SW13 cells. Thus, the binding of BPAG1n to one cytoskeletal network does not preclude its ability to associate with the other. This differs from brain β-spectrin, which in one report appeared to bind either NFs or actin MFs through the ABD (Frappier et al., 1992). Our demonstration that the ABD of BPAG1n associates only with actin filaments and not NFs further underscores this distinction.

More relevant to BPAG1n is that antibodies against plectin partially localize not only to IFs, but also to actin stress fibers and focal contacts in cultured cells (Foisner et al., 1991; Seifert et al., 1992). That plectin may cross-link actin and IF networks has recently been proposed by Foisner et al. (1995), who showed by immunoelectron microscopy that antibodies against plectin label cross-bridge-like structures that connect IFs with actin MFs in cytoskeletal extracts from glioma cells expressing endogenous plectin. While this observation is intriguing, the partial colocalization by immunofluorescence, coupled with the potential for artifacts in in vitro cytoskeletal preparations, has made it difficult to assess whether these cross-bridges exist in vivo, whether they perform a functional role, and whether the interaction, if real, involves direct bridging by a single molecule. The role of this association has been further complicated by studies suggesting that plectin also associates with microtubules and with β-spectrin (Foisner et al., 1991, 1995).

While the role of plectin in the cytoskeleton awaits the generation of plectin null cells or animals, plectin may perform a similar function to BPAG1n. We note here that this seems even more likely given that plectin shares homology between amino acid residues 175–425 and the ABDs of BPAG1n and β-spectrin. In contrast to plectin, however, BPAG1n does not seem to associate appreciably with microtubules, at least in the culture studies described in this report. Whether BPAG1n associates with other proteins, as plectin seems to do, remains to be elucidated.

The *BPAG1* knockout provides direct genetic evidence that BPAG1n performs an essential function in sensory neurons. Our immunohistochemistry and in situ hybridizations reveal that BPAG1n is predominantly in axons and axon termini and not in the cell bodies of sensory neurons. Further, the perturbation seen by electron microscopy in the axonal cytoskeleton of *BPAG1* (−/−) mice strongly implies that BPAG1n performs an actin–NF linkage in vivo and provides a graphic illustration of the vital features of this novel type of cytoskeletal connector protein.

What Is the Function of a Molecule That Can Link Actin to NFs?

BPAG1n now provides a molecular mechanism by which the NF network can be tethered not only to the cortical cytoskeleton, but also to the axoplasmic actin cytoskeleton. Actin antibodies have revealed an array of MFs that underlie the axonal membrane (Hirokawa, 1982; Tsukita et al., 1986). Additionally, Fath and Lasek (1988) have found a lattice of shorter, but abundant actin MFs in the axoplasm of squid DRGs, suggesting that actin MFs play a role in the dynamic architecture of the central axon. It has been widely speculated that the axonal network of actin interacts with microtubules to play a role in vesicle transport (Griffith and Pollard, 1978; Nemhauser and Goldberg, 1985). It may be that in the *BPAG1n* null mice, NFs become disorganized, resulting in perturbations in these connections.

It seems likely that severing the BPAG1n connection between NFs and MFs affects axonal transport. It has already been established that aberrations in motor neuron NFs, similar to the ones we describe for *BPAG1* (−/−) sensory neuron NFs, negatively affect axonal transport (Collard et al., 1995). In addition, we cannot rule out the possibility that the actin cytoskeleton may be perturbed in *BPAG1* (−/−) mice. In this regard, it is interesting that biochemical disruption of MFs also blocks axonal transport (Nemhauser and Goldberg, 1985, and references therein).

It is interesting that the axon termini of certain sensory neurons contain BPAG1n. That BPAG1n function is important in these regions is underscored by the degeneration of muscle spindles and nerve endings in the skin of *BPAG1* (−/−) mice (Guo et al., 1995; Sotelo and Guenet, 1988). Although terminal boutons of parasympathetic and motor axons have few if any NFs (Lasek and Hoffman, 1976), the sensory axon termini at muscle spindles and in skin may be more similar to the extensively branched preterminal regions of parasympathetic axons, which are rich in NFs (Paggi and Lasek, 1987). Finally, it is intriguing that muscle spindles depend upon their sensory nerves (and not their motor nerves) for development and survival during the first 2 weeks after birth (Zelena and Soukup, 1974), providing a partial explanation as to why motor dysfunction occurs in the *BPAG1* knockout mice. To what extent BPAG1n may perform multifaceted functions in the axons and axon termini will need to be explored in more detail in the future.

Why Would Disrupting the Linkage between Actin and NF Selectively Kill Sensory Neurons?

If BPAG1n provides a linkage between MFs and NFs, when are these linkages formed and are they more important to sensory neurons than to other neurons? The *BPAG1* (−/−) phenotype indicates that the attachment is most needed following stable synapse formation in postnatal axons and preterminal axon branches. Whether the attachment is inhibitory to migrating neurons, either developmentally or in response to injury, will be of interest to address in the future, as is the issue of how BPAG1n is prevented from associating with the actin cytoskeleton in DRG perikarya where it is first synthesized.

It is perplexing that BPAG1n is not comparably expressed in motor neurons. Sensory neurons can vary dramatically in size, myelination, and axonal transport rates, and hence any of these properties alone is unlikely to account for this difference. Perhaps BPAG1n is a member of a larger family of actin–IF linker molecules

and a gene product, possibly plectin, may perform the functions of BPAG1n in motor neurons. Alternatively, the ability to tether NFs to MFs may be an intrinsic property of sensory neurons. The NF network of cultured motor, but not sensory, neurons collapses upon microinjection of SMI 31 antibody against phosphorylated NF-H (Durham, 1992), suggesting that the IF cytoskeleton of motor neurons might be selectively more fragile than that of sensory neurons. While future studies will be necessary to assess whether this is the case, this could also explain why mutations in NF genes give preferential loss of motor, but not sensory, neurons in transgenic mice (Cote et al., 1993; Xu et al., 1993). These results have important implications for our understanding not only of the role of actin–IF associations in vivo, but also of the source of neuronal degeneration in *BPAG1* null mice and in related human neurodegenerative disorders.

Experimental Procedures

Generation of BPAG1n Antibodies

Preimmune sera were screened for their failure to bind to mouse brain and skin extracts. Rabbits were then injected with a GST fusion protein containing in-frame amino acid residues 31–470 of BPAG1n1. Protein was purified using binding to GSH-conjugated Sepharose beads, and FPLC anion affinity chromatography (Kouklis et al., 1994). A 250 μg injection was followed by two boosts of 150 μg. Antisera were affinity purified by passage through GST and GST–BPAG1n Sepharose columns.

Construction of pFG-BPtail, pBPabd-FG, and pBPAG1n and Transfections

To make pFG-BPtail, sequences encoding the 768 amino acid tail of human BPAG1 (residues 2201–2649 of BPAG1e) were subcloned in-frame at the EcoRI site of pECE-FLAG, a mammalian expression vector containing the SV40 major early promoter and enhancer, an encoded 9 amino acid residue FLAG (FG) epitope tag at the 5′ end, and the SV40 polyadenylation signal at the 3′ end (provided by Dr. Magnus Pfahl, La Jolla Cancer Research Foundation, La Jolla, CA). Sequences encoding the 464 amino acid ABD of human BPAG1n with an engineered FLAG epitope tag at its carboxyl terminus were subcloned into the NotI–XbaI site of plasmid pECE-FLAG (pBPabd-FG), and sequences encoding full-length human BPAG1n1 were subcloned into the NotI–SacI site of this vector (pBPAG1n) (the endogenous FLAG is not utilized in these constructs).

Acknowledgments

Correspondence should be addressed to E. F. A special thank you goes to Dr. Robert Wollman (Department of Neurology, University of Chicago) for providing some of the electron micrographs of *BPAG1* null mice and for his valuable discussions on neuropathology. We also thank Dr. Su Hao Lo in our lab for his advice in conducting the actin binding studies and for providing us with the tensin ABD protein. We thank Zhao-hui Yang for his helpful advice concerning various aspects of molecular biology, Dr. Paul Janmey (Harvard Medical School) for providing us with purified actin, and Dr. Jouni Uitto (Thomas Jefferson University) for providing us with cDNA clones for BPAG1e. We thank Dr. Hashimoto (Keio University School of Medicine, Japan) for his kind gift of m5e antibody, Dr. Chloe Bulinski for her gift of anti-tubulin antibody, Dr. Robert Evans (University of Colorado Health Science Center, Denver) for his kind gift of SW13 cells, and Dr. Liliana Minichiello and Dr. Rudiger Klein (Heidelberg, Germany) for their gift of the *trkC* cDNA. We thank Dr. Uhna Sung for her work on BPAG1e while she was in our laboratory. During this time, she prepared some of the *BPAG1e* cDNAs and expression vectors used in our studies. Finally, we thank Ms. Linda Degenstein for her help and assistance with the mice used in these studies. This work was supported by a grant from the National Institutes of Health (R01-AR27883). E. F. is an Investigator of the Howard Hughes Medical Institute (HHMI). Y. Y. is a research associate of the HHMI. J. D. is an MD/PhD predoctoral student supported by the Medical Scientist Training Program, which is funded by the National Institutes of Health.

Received March 28, 1996; revised July 1, 1996.

References

Albers, K., and Fuchs, E. (1987). The expression of mutant epidermal keratin cDNAs transfected in simple epithelial and squamous cell carcinoma lines. J. Cell Biol. *105*, 791–806.

Brown, A., Bernier, G., Mathieu, M., Rossant, J., and Kothary, R. (1995a). The mouse dystonia musculorum gene is a neural isoform of bullous pemphigoid antigen 1. Nature Genet. *10*, 301–306.

Brown, A., Dalpe, G., Mathieu, M., and Kothary, R. (1995b). Cloning and characterization of the neural isoforms of human dystonin. Genomics *29*, 777–780.

Campbell, R.M., and Peterson, A.C. (1992). An intrinsic neuronal defect operates in dystonia musculorum: a study of *dt*/*dt*↔+/+ chimeras. Neuron *9*, 693–703.

Collard, J.-F., Cote, F., and Julien, J.-P. (1995). Defective axonal transport in a transgenic mouse model of amyotrophic lateral sclerosis. Nature *375*, 61–64.

Cote, F., Collard, J.-F., and Julien, J.-P. (1993). Progressive neuropathy in transgenic mice expressing the human neurofilament heavy gene: a mouse model of amyotrophic lateral sclerosis. Cell *73*, 35–46.

Coulombe, P.A., Hutton, M.E., Letai, A., Hebert, A., Paller, A.S., and Fuchs, E. (1991). Point mutations in human keratin 14 genes of epidermolysis bullosa simplex patients: genetic and functional analyses. Cell *66*, 1301–1311.

Duchen, L.W. (1976). Dystonia musculorum: an inherited disease of the nervous system in the mouse. Adv. Neurol. *14*, 353–365.

Durham, H.D. (1992). An antibody against hyperphosphorylated neurofilament proteins collapses the neurofilament network in motor neurons but not in dorsal root ganglion cells. J. Neuropathol. Exp. Neurol. *51*, 287–297.

Fath, K.R., and Lasek, R.J. (1988). Two classes of actin microfilaments are associated with the inner cytoskeleton of axons. J. Cell Biol. *107*, 613–621.

Foisner, R., Traub, P., and Wiche, G. (1991). Protein kinase A- and protein kinase C-regulated interaction of plectin with lamin B and vimentin. Proc. Natl. Acad. Sci. USA *88*, 3812–3816.

Foisner, R., Bohn, W., Mannweiler, K., and Wiche, G. (1995). Distribution and ultrastructure of plectin arrays in subclones of rat glioma C_6 cells differing in intermediate filament protein (vimentin) expression. J. Struct. Biol. *115*, 304–317.

Frappier, T., Derancourt, J., and Pradel, L.-A. (1992). Actin and neurofilament binding domain of brain spectrin β subunit. Eur. J. Biochem. *205*, 85–91.

Green, K.J., Virata, M.L.A., Elgart, G.W., Stanley, J.R., and Parry, D.A.D. (1992). Comparative structural analysis of desmoplakin, bullous pemphigoid antigen and plectin: members of new gene family involved in organization of intermediate filaments. Int. J. Biol. Macromol. *14*, 145–153.

Griffith, L., and Pollard, T. (1978). Evidence for actin filament-microtubule interaction mediated by microtubule-associated proteins. J. Cell Biol. *78*, 958–965.

Guo, L., Degenstein, L., Dowling, J., Yu, Q.-C., Wollmann, R., Perman, B., and Fuchs, E. (1995). Gene targeting of *BPAG1*: abnormalities in mechanical strength and cell migration in stratified squamous epithelia and severe neurologic degeneration. Cell *81*, 233–243.

Hirokawa, N. (1982). Cross-linker system between neurofilaments, microtubules, and membranous organelles in frog axons revealed by the quick-freeze, deep-etching method. J. Cell Biol. *94*, 129–142.

Hopkinson, S.B., and Jones, J.C.R. (1994). Identification of a second protein product of the gene encoding a human epidermal autoantigen. Biochem. J. *300*, 851–857.

Kothary, R., Clapoff, S., Brown, A., Campbell, R., Peterson, A., and Rossant, J. (1988). A transgene containing lacZ inserted into the dystonia locus is expressed in neural tube. Nature *335*, 435–437.

Kouklis, P., Hutton, E., and Fuchs, E. (1994). Making the connection: keratin intermediate filaments and desmosomes proteins. J. Cell Biol. *127*, 1049–1060.

Lasek, R.J., and Hoffman, P.N. (1976). The neuronal cytoskeleton, axonal transport and axonal growth. Cold Spring Harbor Confer. Cell Prol. *3*, 1021–1049.

Lee, M.K., Xu, Z., Wong, P.C., and Cleveland, D.W. (1993). Neurofilaments are obligate heteropolymers *in vivo*. J. Cell Biol. *122*, 1337–1350.

Lersch, R., Stellmach, V., Stocks, C., Giudice, G., and Fuchs, E. (1989). Isolation, sequence, and expression of a human keratin K5 gene: transcriptional regulation of keratins and insights into pairwise control. Mol. Cell. Biol. *9*, 3685–3697.

Lo, S.H., Janmey, P.A., Hartwig, J.H., and Chen, L.B. (1994). Interactions of tensin with actin and identification of its three distinct actin-binding domains. J. Cell Biol. *125*, 1067–1075.

Minichiello, L., Piehl, F., Vazquez, E., Schimmang, T., Hokfelt, T., Represa, J., and Klein, R. (1995). Differential effects of combined trk receptor mutations on dorsal root ganglion and inner ear sensory neurons. Development *121*, 4067–4075.

Nemhauser, I., and Goldberg, D.J. (1985). Structural effects in axoplasm of DNase I, an actin depolymerizer that blocks fast axonal transport. Brain Res. *334*, 47–58.

Paggi, P., and Lasek, R.J. (1987). Axonal transport of cytoskeletal proteins in oculomotor axons and their residence times in the axon terminals. J. Neurosci. *7*, 2397–2411.

Seifert, G.J., Lawson, D., and Wiche, G. (1992). Immunolocalization of the intermediate filament-associated protein plectin at focal contacts and actin stress fibers. Eur. J. Cell Biol. *59*, 138–147.

Sotelo, C., and Guenet, J.L. (1988). Pathologic changes in the CNS of dystonia musculorum mutant mouse: an animal model for human spinocerebellar ataxia. Neuroscience *27*, 403–424.

Stanley, J.R. (1993). Cell adhesion molecules as targets of autoantibodies in pemphigus and pemphigoid, bullous diseases due to defective epidermal cell adhesion. Adv. Immunol. *53*, 291–325.

Stappenbeck, T.S., and Green, K.J. (1992). The desmoplakin carboxyl terminus coaligns with and specifically disrupts intermediate filament networks when expressed in cultured cells. J. Cell Biol. *116*, 1197–1209.

Sternberger, L.A., and Sternberger, N.H. (1983). Monoclonal antibodies distinguish phosphorylated and nonphosphorylated forms of neurofilaments *in situ*. Proc. Natl. Acad. Sci. USA *80*, 6126–6130.

Sugi, T., Hashimoto, T., Hibi, T., and Nishikawa, T. (1989). Production of human monoclonal anti-basement membrane zone (BMZ) antibodies from a patient with bullous pemphigoid (BP) by Epstein-Barr virus transformation. J. Clin. Invest. *84*, 1050–1055.

Tamai, K., Sawamura, D., Do, H.C., Tamai, Y., Li, K., and Uitto, J. (1993). The human 230-kD bullous pemphigoid antigen gene (BPAG1): exon-intron organization and identification of regulatory tissue specific elements in the promoter region. J. Clin. Invest. *92*, 814–822.

Tsukita, S., Tsukita, S., Kobyayashi, T., and Matsumoto, G. (1986). Subaxolemmal cytoskeleton in squid giant axon. II. Morphological identification of microtubule and microfilament-associated domains of axolemma. J. Cell Biol. *102* 1710–1725.

Xu, Z., Cork, L.C., Griffin, J.W., and Cleveland, D.W. (1993). Increased expression of neurofilament subunit NF-L produces morphological alterations that resemble the pathology of human motor neuron disease. Cell *73*, 23–33.

Yang, X.W., Zhong, R., and Heintz, N. (1996). Granule cell specification in the developing mouse brain as defined by expression of the zinc finger transcription factor RU49. Development *122*, 555–566.

Zelena, J., and Soukup, T. (1974). The differentiation of intrafusal fibre types in rat muscle spindles after motor denervation. Cell Tissue Res. *153*, 115–136.